Light scattering by cholesteric skyrmions

G. De Matteis,[1,2,4,*] D. Delle Side,[1,†] L. Martina,[1,3,4,‡] and V. Turco[1,3,§]

[1]*Dipartimento di Matematica e Fisica, Università del Salento, C.P. 193 I-73100 Lecce, Italy*

[2]*Istituto di Istruzione Secondaria Superiore "V. Lilla" MIUR - Italian Ministry of Education and Research, Francavilla Fontana (BR) I-72021, Italy*

[3]*INFN, Sezione di Lecce Via per Arnesano, C.P. 193 I-73100 Lecce, Italy*

[4]*GNFM-INDAM, Città Universitaria - P.le Aldo Moro 5, C.P. 00185 Roma, Italy*

We study the light scattering by localized quasiplanar excitations of a cholesteric liquid crystal known as spherulites. We quantitatively evaluate the cross section of the axis rotation for polarized light by taking into account the anisotropic optical properties of the medium and the peculiar shape of the excitations. Because of the complexity of the system under consideration, we exploit also a simplified analytical description of the spherulite and evaluate the scattering cross sections in the Born approximation. We compare the scattering data by the analytical and the numerical skyrmion solutions for several choices of the model parameters. The effects of changing values of the driving external static electric (or magnetic) field is also considered. Possible applications of the phenomenon are envisaged.

I. INTRODUCTION

In the past few years great efforts have been made to develop new materials for optoelectronics and photonics applications. A relevant role in this work has been played by liquid crystals (LC) physics [1,2] for a quite a long time. In fact, nowadays LC are widely used in all types of display applications and, in addition, their unique nonlinear electro-optical properties make them suitable material for nondisplay applications [3,4], like optical filters and switches, beam-steering devices, spatial light modulators, lasers, optical wave-guiding, and nonlinear components. On the other hand, there is also wide interest on a variety of new textures appearing both in quasi-two-dimensional (2D) layers of chiral liquid crystals (CLCs) like two-dimensional *cholesteric fingers* [5], and 3D ones, like *cholesteric bubbles* or *spherulites* [6–8] and *nematicons* [9]. On the experimental side, Carboni *et al.* [10] detected a phase transition between the finger and the skyrmion textures, strongly depending on the thickness of the confining cell. They showed that the texture changes are driven by temperature through a parameter ζ proportional to the thickness and to a proper chirality parameter. Moreover, Smalyukh *et al.* recently generated a new type of defects in the director field configurations, called *triple-twisted torons* (T3s), by geometrical frustration and by using Laguerre-Gaussian vortex laser beams. They also showed numerically their existence [11,12], but here we will not consider such type of textures.

Spherulites have been studied from a theoretical point of view in Refs. [13,14] and here we consider them for their potential optotechnological applications. Spherulites in CLCs share some properties with the 2D skyrmions in magnetic systems [15,16] and can be derived in the framework of the Frank-Oseen continuum theory [17,18]. By applying external fields and imposing homeotropic anchoring boundary conditions (BCs) [19,20], the free helicoidal equilibrium configurations can be deformed into the isolated axisymmetric skyrmionic structures [21,22], stabilized by the underlying molecular chirality and boundary conditions, which in turn reflect into topological conservation laws. However, they are very sensitive to the external fields and may possess slow modulations in certain preferred direction. The theory also describes the cholesteric fingers [23,24], or helicoids, with disclination-type defects, which can be described, at least in some approximate settings, in terms of integrable nonlinear equations [25,26], stabilized both by topological and nontopological conservation laws. This does not seem to be the case for the spherulites, which we investigated under this aspect in Ref. [14].

More recently, in Ref. [27], Smalyukh *et al.* have reviewed the spontaneous and optical generation of several types of defects in CLCs, classifying them by their topological charge and the kind of disclinations they exhibit. In detail, they observed the above-mentioned structures through confocal and standard polarized microscopy techniques. They presented both the vertical and in-plane cross-sectional images and 3D reconstructions of the defects. They exhibited direct observations and schematic representations of a topological defect similar to the one obtained in Refs. [13,14] in both the XY and XZ plane projections. From our point of view, this latter result is particularly significant, since we would like to study it on a theoretical basis. Those studies are extended and complemented by a wide set of investigations, both on the theoretical and experimental, which have been devoted to the subject of localized configurations appearing in CLCs under several external conditions [26,28,29]. However, so far,

*giovanni.dematteis@istruzione.it

†nico.delleside@unisalento.it

‡martina@le.infn.it

§vito.turco@le.infn.it

the light scattering from helicoidal CLC structures has been studied only in the bulk [30,31] and, in confined geometries like thin films or droplets, it has been considered only on the experimental side [32–34].

Thus, the aim of the present paper is to characterize, from the basic principles, the main properties of the scattering of light, propagating into a CLCs layer, by an isolated spherulite. Assuming a constant value of the temperature and of the spontaneous chirality, the external factors, as the thickness, the anchoring interactions, and the external electric and magnetic fields, are the controlling parameters for the investigated phenomena. These properties may suggest better control of the spherulites' optical properties and their possible applications.

Very recently, the authors of Ref. [35] investigated numerically the optical properties of a hexagonal half-skyrmion lattice in confined CLCs, and they found resonant structures in the reflectivity. However, we notice that the physical setting considered in that work is quite different from ours, since they took into account the scattering along the axis of the skyrmion. Here we consider the interaction of an isolated spherulite with light propagating transversally to its axis.

The present paper is organized as follows. In Sec. II we introduce the continuum elastic model of the CLC, and we obtain the corresponding equilibrium equations and analyze the skyrmion (spherulite) solutions, either by analytical or numerical methods. In Sec. III we address the problem of light scattering in the plane orthogonal to the axis of a spherulite. In Sec. IV we provide perturbative solutions for the light-scattering equations in a Born approximation. In particular in Sec. IV A we compute the cross section of the conversion process of incoming polarized light in the incidence plane into the outgoing polarized light in the perpendicular direction. Analogously, in Sec. IV B we consider the complementary problem of the change of polarization axis from the orthogonal direction to the liquid crystal to the a planar direction. Finally, in the Conclusions we summarize our results and address some possible experimental realizations.

II. SKYRMIONS IN CHIRAL LIQUID CRYSTALS

A LC is described by a unimodular director field $\mathbf{n}(\mathbf{r})$ belonging to $\mathbb{RP}^2$ [17,18], which in polar representation is given by

$$\mathbf{n}(\mathbf{r}) = \sin\theta(\mathbf{r})(\cos\psi(\mathbf{r})\mathbf{i} + \sin\psi(\mathbf{r})\mathbf{j}) + \cos\theta(\mathbf{r})\mathbf{k}. \quad (2.1)$$

In the bulk a CLC director field $\mathbf{n}(\mathbf{r})$ is governed by the Frank-Oseen free-energy density

$$\begin{aligned}
\omega_{\mathrm{FO}} = &\frac{K_1}{2}(\nabla \cdot \mathbf{n})^2 + \frac{K_2}{2}(\mathbf{n} \cdot \nabla \times \mathbf{n} - q_0)^2 \\
&+ \frac{K_3}{2}(\mathbf{n} \times \nabla \times \mathbf{n})^2 \\
&+ \frac{(K_2 + K_4)}{2}\nabla \cdot [(\mathbf{n} \cdot \nabla)\mathbf{n} - (\nabla \cdot \mathbf{n})\mathbf{n}] - \frac{\varepsilon}{2}(\mathbf{n} \cdot \mathbf{E})^2,
\end{aligned}$$
$$(2.2)$$

where q_0 is the chirality parameter of the cholesteric phase and the positive reals K_1, K_2, K_3, and K_4 are the Frank elastic constants, which we set to be $K_1 = K_2 = K_3 = K$ and $K_4 = 0$ for sake of simplicity. The last term in (2.2) represents

the interaction energy density with an external static electric field $\mathbf{E}$ (here supposed to be spatially uniform along the $\mathbf{k}$ direction) or, equivalently, a magnetic field $\mathbf{H}$. Of course, in the presence of the external electric (magnetic) field, the general rotational symmetry is broken and reduced to rotations around the direction of $\mathbf{E}$ ($\mathbf{H}$). In the absence of anchoring conditions, the field $\mathbf{n}(\mathbf{r})$ would form a cholesteric helix with the axis orthogonal to $\mathbf{E}$ ($\mathbf{H}$). However, supposing the CLC confined within a layer $\mathcal{B} = \{(x, y, z) \in \mathbb{R}^3, |z| \leqslant \frac{L}{2}\}$, also the translational symmetry in the direction of $\mathbf{k}$ is broken and the interaction of the CLC with the planar bounding surfaces can be encoded by the additional Rapini and Papoular surface energy contribution [36]

$$\omega_s = \tfrac{1}{2}K_s[1 + \alpha(\mathbf{n} \cdot \boldsymbol{\nu})^2], \quad (2.3)$$

where $K_s > 0$, $\alpha > 0$, and $\boldsymbol{\nu}$ is the unit outward normal to the boundary surface. Strong homeotropic anchoring is obtained for $K_s \to \infty$, which corresponds to the Dirichlet boundary conditions $\mathbf{n}(x, y, z \pm \frac{L}{2}) = \mathbf{k}$. So helices are deformed and confined within $\mathcal{B}$: Extended structures called helicoids (or helicons and, sometimes, *fingers*) or localized spherulites (also *skyrmions*) may form, depending on the existence or not of a preferred direction in the perturbation of $\mathbf{n}$.

In order to find equilibrium configurations of the CLC we have to minimize the Frank-Oseen free energy plus a surface term, under the appropriate boundary conditions at infinity. We choose to limit ourselves to axisymmetric isolated solutions. More precisely, we assume $\theta = \theta(\rho, z)$ and $\psi = \psi(\phi)$, where ρ, z, and ϕ are the usual cylindrical coordinates around the axis $\mathbf{k}$. Very recently, in Ref. [25] the authors considered the more general case of the azimuthal angle ψ depending also on ρ and z, and, accordingly, they numerically minimized the free energy (2.2) in order to find axysimmetric solutions. On the other hand, for the purpose of the optical phenomena analyzed in this paper, the above ansatz is sufficiently reasonable, also in order to comply with the simplifying hypothesis (v) made in Sec. 3. Under our assumptions, the Euler-Lagrange equations for the fields θ and ψ are

$$\begin{aligned}
\theta_{\rho\rho} + \theta_{zz} + \frac{1}{\rho}\theta_\rho + \frac{1}{\rho}q_0\sin(\phi - \psi)(\psi_\phi\cos 2\theta - 1) \\
+ \frac{\psi_\phi^2\sin 2\theta}{2\rho^2} - \frac{\varepsilon E^2}{2K}\sin 2\theta = 0
\end{aligned}$$
$$(2.4)$$

and

$$2\frac{\sin^2\theta}{\rho^2}\psi_{\phi\phi} - 2q_0\left(\theta_\rho + \frac{1}{2}\frac{\sin 2\theta}{\rho}\right)\cos(\psi - \phi) = 0. \quad (2.5)$$

The compatibility of systems (2.4) and (2.5) is provided by setting

$$\psi(\phi) = \phi \pm \frac{\pi}{2}, \quad \phi \in [0, 2\pi]. \quad (2.6)$$

Without losing generality, we choose the positive determination in the previous equation. Accordingly, the director field takes the simpler form

$$\begin{aligned}
\mathbf{n} &= \mathbf{n}(\rho, \phi, z) = \cos\theta(\rho, z)\mathbf{k} + \sin\theta(\rho, z)\boldsymbol{\phi}, \\
\boldsymbol{\phi} &= -\sin\phi\mathbf{i} + \cos\phi\mathbf{j}
\end{aligned}$$
$$(2.7)$$

and all the admissible equilibrium configurations are solutions of the boundary value problem (BVP) in dimensionless variables

$$\frac{\partial^2 \theta}{\partial z^2} + \frac{\partial^2 \theta}{\partial \rho^2} + \frac{1}{\rho}\frac{\partial \theta}{\partial \rho} - \frac{1}{\rho^2}\sin\theta\cos\theta \mp \frac{4\pi}{\rho}\sin^2\theta$$
$$- \pi^4\left(\frac{E}{E_0}\right)^2\sin\theta\cos\theta = 0, \tag{2.8}$$

$$\theta(0, z) = \pi, \quad \theta(\infty, z) = 0,$$

$$\partial_z\theta\left(\rho, \pm\frac{\nu}{2}\right) = \mp 2\pi k_s \sin\theta\left(\rho, \pm\frac{\nu}{2}\right)\cos\theta\left(\rho, \pm\frac{\nu}{2}\right), \tag{2.9}$$

where the lengths are rescaled with respect to the so-called pitch length $p = \frac{2\pi}{|q_0|}$. Here $E_0 = \frac{\pi\ |q_0|\ }{2}\sqrt{\frac{K}{\varepsilon}}$ is the critical unwinding field for the cholesteric-nematic transition in nonconfined CLCs [37], $\nu = L/p$ is the normalized thickness of the layer, and $k_s = K_s/(Kq_0)$ the rescaled strength of the interaction liquid-boundary surfaces. The $\mp$ sign in Eq. (2.8) reflects the sign of q_0: In the following we take $q_0 < 0$, with no loss of generality. Finally, it is convenient to simplify the notation by setting $\frac{1}{\rho_1} = \pi^2\frac{E}{E_0}$, an adimensional parameter which measures the relative strength of the electric field with respect to the critical one. Systems (2.8) and (2.9) are a 3D perturbed sine-Gordon-type equation: Chirality and BCs do not allow integration in analytical form. The main deformation comes from the fifth term in (2.8), associated to the chirality of the system.

However, to get information about the shape of a spherulite, one can evaluate the asymptotic behavior of the solutions near $\rho \to 0$ and $\rho \to \infty$ for the pure cylindrical reduction of (2.8), i.e., $\theta_z = 0$, which holds when ν is sufficiently large and modulations in the z variable are discarded.

Near $\rho \to 0$ both the chiral and the electric interaction can be neglected with respect to the other terms. Thus setting both $q_0 = 0$ and $E = 0$, Eq. (2.8) reduces to the conformally invariant O(3)-sigma model in polar representation [38] whose solution is the Belavin-Polyakov one [39], namely

$$\theta = \arccos\left(\frac{\tilde\rho^2 - 4}{\tilde\rho^2 + 4}\right), \quad \tilde\rho = \frac{\rho}{\rho_0}, \tag{2.10}$$

where ρ_0 is an arbitrary scale factor which will be fixed by the breaking terms of the conformal symmetry, namely the fourth and the fifth terms in (2.8). Thus, substituting solution (2.10) into Eq. (2.8) we obtain the estimation

$$\rho_0 = \frac{4}{\pi^3}\left(\frac{E_0}{E}\right)^2 = 4\pi\rho_1^2, \tag{2.11}$$

which can be interpreted as the typical scale of a spherulite, and at the lowest order the solution of (2.8) and (2.9) is approximated by

$$\theta(\rho) = \pi - \frac{\rho}{\rho_0} + O\left[\left(\frac{\rho}{\rho_0}\right)^3\right]. \tag{2.12}$$

Following Ref. [13], in order to describe z modulations, we assume a rough approximation of the solution by deforming
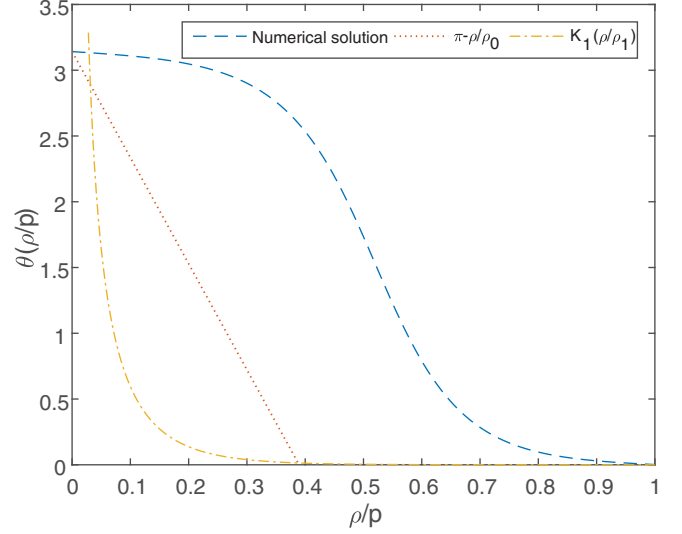

FIG. 1. Comparison for $\frac{E}{E_0} = 1.02$ among the numerical solution of (2.8), the linearly piecewise approximation (2.12), and the analytic solution of the linearized equation.

(2.12) as

$$\theta(\rho, z) = \begin{cases} \pi - \frac{\rho}{\rho_0 Z(z)} & \rho/Z(z) < \pi\rho_0 \\ 0 & \rho/Z(z) > \pi\rho_0 \end{cases}. \tag{2.13}$$

Replacing (2.13) into the Frank-Oseen energy and minimizing it, one gets the following z modulation:

$$Z(z) = 1 - \frac{2\pi k_s \cosh\left(\frac{z}{\rho_1}\right)}{2\pi k_s \cosh\left(\frac{\nu}{2\rho_1}\right) + \frac{1}{\rho_1}\sinh\left(\frac{\nu}{2\rho_1}\right)}. \tag{2.14}$$

We note that the sizes of the vortices decrease as $|z|$ and k_s increase. However, we remark that numerical calculations show that the function $Z(z)$ in (2.14) does not fit accurately the actual behavior of the solutions, except for high external electric fields E, whose effects are much stronger than those related to the anchoring k_s.

In the asymptotic limit $\rho \to \infty$ the dominant term comes from the external electric field, which affects the shape of skyrmion by the reduced equation

$$\frac{\partial^2 \theta}{\partial \rho^2} + \frac{1}{\rho}\frac{\partial \theta}{\partial \rho} - \frac{1}{2\rho_1^2}\sin 2\theta = 0, \tag{2.15}$$

which is known as cylindrical sine-Gordon equation [40]. The most relevant fact about this equation is its connection with the celebrated Painlevé III equation [14,41,42] (see also Ref. [43], chap. 32), and thus it can be analytically solved. However, in correspondence to the boundary conditions at ∞ stated in (2.9), this equation has always singular solutions at $\rho \to 0$. Thus the validity of such an approximation is limited to a neighborhood of ∞, where its asymptotics is the same as for the first-order modified Bessel functions of second kind, namely

$$\theta \rightsquigarrow c_2\sqrt{\frac{\rho_1}{\rho}}\exp\left[-\frac{\rho}{\rho_1}\right]. \tag{2.16}$$

The above results give us useful indications about the shape of the spherulite or skyrmion, but many important details
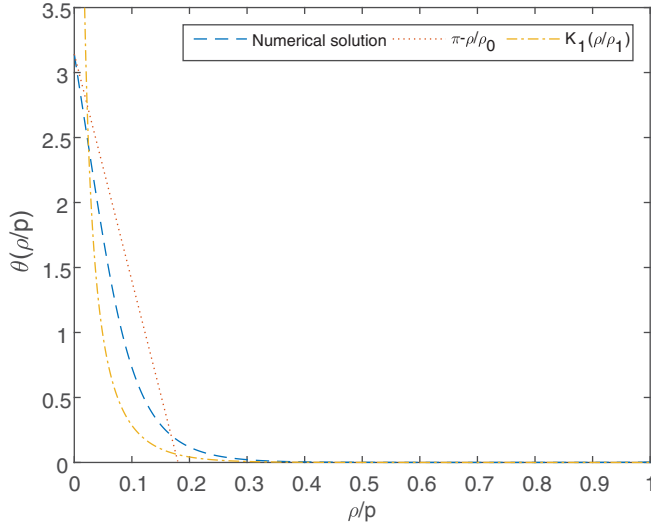
FIG. 2. Comparison for $\frac{E}{E_0} = 1.5$ among the numerical solution of (2.8), the linearly piecewise approximation (2.12), and the analytic solution of the linearized equation.

are missed. In fact, to have a good account of them and to estimate the goodness of the approximations made above, we need to perform numerical calculations on the BVP (2.8) and (2.9). To this aim, we use the standard central finite-difference discretization and the Newton-Raphson method [44,45], initialized by the shooting method for the planar reduction of the system (i.e., $\theta_z = 0$).

It turns out that for sufficiently large electric fields, i.e., $\frac{E}{E_0} > 1$ the linear approximations matches with the numerical solution quite closely, as represented in Fig. 1. On the other hand, the approximations become very rough for relatively weak fields, i.e., $\frac{E}{E_0} \approx 1$, as shown in Fig. 2. As far as the numerical cases considered in the present work, this behavior denotes the underestimation of the chiral term in the linear approximation, in particular at the intermediate scales $\rho_1 \leqslant \rho \leqslant \rho_0$. The numerical solutions of the BVP (2.8) for different values of the couple $(\frac{E}{E_0}, k_s)$ are depicted in Figs. 3

and 4. In each figure the profiles $\theta(\rho)$ for different values of $z \in [-\nu/2, \nu/2]$ are represented. We note that when the strength of the anchoring is small, the profiles are almost the same for every value of coordinate z. This means that when the interfaces at the boundaries of the cell have a really small homeotropic effect on the director's configuration, a quasiperfect cylindrical shape holds for axisymmetric solutions. In this case, the planar vortices described by $\theta(\rho)$ have the same, maximum, size for every value of z. However, if we impose a quite stronger homeotropic effect at the boundaries, then the vortices tend to have a reduced size, which becomes smaller as $|z|$ reaches the value $\frac{\nu}{2}$. We stress that for greater external fields the size of all vortices narrows. This provides the main features of the spherulites which we will exploit in next section, when considering the light scattering by such a type of defects in a CLC. More details are given in Ref. [14]. A 3D representation of the texture of a spherulite or skyrmion is given in Fig. 5 for a particular choice of the parameters.

III. SCATTERING OF LIGHT ON A CLC CYLINDRICAL STRUCTURE

In this section we consider the scattering of an electromagnetic (e.m.) wave, propagating through a confined CLC, which is under the suitable conditions for a spherulite to be formed. The geometry is the same as in the previous section, as the same is the choice of the Cartesian axes. We assume that the wave vector of the incoming field is parallel to the (x, y) plane. The propagation of the wave is described in terms of the oscillating electric field $\vec{E}$, to be distinguished from the static electric field $\mathbf{E}$, and by the associated electric displacement field $\vec{D}$ via the equation [46]

$$\nabla(\nabla \cdot \vec{E}) - \nabla^2 \vec{E} = -\partial_{tt}\vec{D}. \tag{3.1}$$

As usual, this equation has been obtained by substituting the magnetic field by the Maxwell equations. The electric anisotropy of the CLC is made explicit by the existence of a permeability tensor, which locally has an orthogonal component $\epsilon_\perp$ if $\vec{E} \perp \mathbf{n}$ and a parallel one $\epsilon_\parallel$ if $\vec{E} \parallel \mathbf{n}$. Then the costitutive relation is given by [17,18,47]

$$\vec{D} = \epsilon_\perp \vec{E} + \Delta\epsilon \, \mathbf{n}(\vec{E} \cdot \mathbf{n}), \quad \Delta\epsilon = \epsilon_\parallel - \epsilon_\perp. \tag{3.2}$$
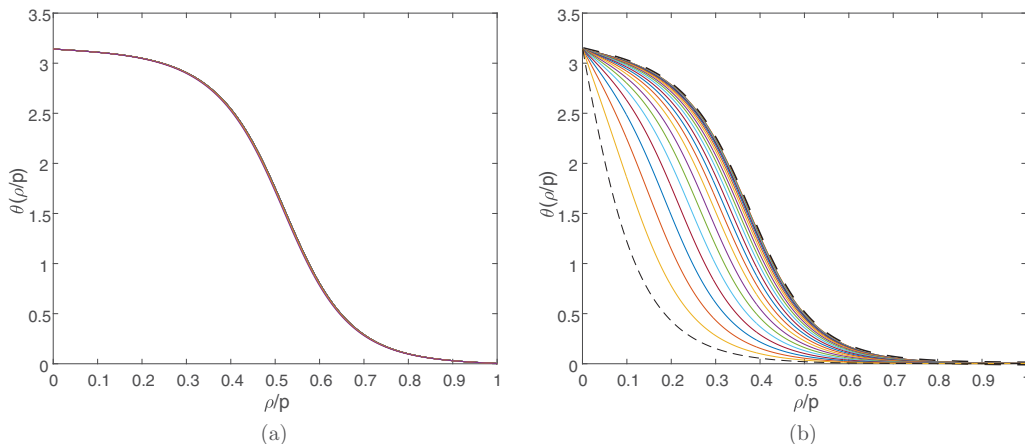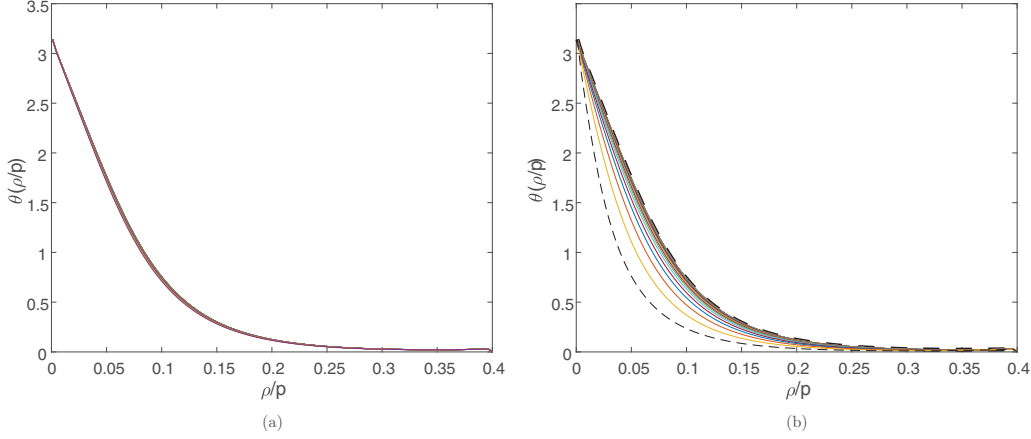

(a)

(b)

FIG. 3. Profiles $\theta(\rho)$ for $E/E_0 = 1.02$, $k_s = 0.1$ (a), and $k_s = 6$ (b). Different curves refer to different values of $|z|$. Dashed curves have to be referred to $z = 0$ (the thin one) and to $|z| = \nu/2$ (the thicker one).

FIG. 4. Profiles $\theta(\rho)$ for $E/E_0 = 1.5$, $k_s = 0.1$ (a), and $k_s = 6$ (b). Different curves refer to different values of $|z|$. Dashed curves have to be referred to $z = 0$ (the thin one) and to $|z| = \nu/2$ (the thicker one). We note that the effect of a greater external electric field is to narrow the size of the vortices for fixed values of k_s.

Here both $\epsilon_\perp$ and $\epsilon_\parallel$ are independent of the electric field strength E, so that $\vec{D}$ is a linear function of $\vec{E}$. Let us assume that the incident wave is described by the electric field

$$\vec{E} \rightsquigarrow E_y \, e^{\iota(kx-\omega t)}\mathbf{j} + e^{\iota(\tilde{k}x-\omega t)}\mathbf{k} = \vec{\mathcal{E}}_\infty e^{-\iota\omega t} \qquad x \to -\infty, \tag{3.3}$$

where $k = \frac{\omega}{c}\sqrt{\epsilon_\perp}$ and $\tilde{k} = k\sqrt{1 + \frac{\Delta\epsilon}{\epsilon_\perp}}$.

We suppose that the spherulite is not perturbed by the wave, but we need to assume certain supplementary conditions:

(i) the liquid crystal molecules are not deformed or rotated by the wave, which implies $\omega \gg \frac{1}{\tau}$, τ being any "relaxation time" of the CLC.

(ii) We assume that the wavelength λ is comparable with ρ_0 or smaller [i.e., $k(\omega) \gtrsim \frac{1}{\rho_0}$], ρ_0 being the typical spherulite size defined in Eq. (2.11).

(iii) We assume that the effects of the bounding surfaces are negligible while calculating solutions of Eq. (3.1).

(iv) A strong supplementary condition we introduce is $\nabla \cdot \vec{E} = 0$, which may imply $\nabla \cdot \vec{D} = \rho_{\text{free}} \neq 0$ somewhere in the domain, especially in the core of the spherulites, where we expect significant variations of the fields. However, at this stage of our analysis we prefer to adopt such an assumption, because, by this way, the equations can be considered a 0-order approximation. Then an *a posteriori* evaluation of the local free charge density will clarify how good our hypothesis is.

(v) A final remark concerns the functional dependence of the shape of the spherulite, which we assume to be simply $\theta = \theta(\rho)$. Thus, for sake of simplicity we neglect the modulation along the z axis described by (2.14). Also in this case higher-order corrections should be considered later.

Under the conditions above, for the enveloping field $\vec{\mathcal{E}} = \vec{\mathcal{E}}(\vec{r})$ Eq. (3.1) becomes

$$\nabla^2 \vec{\mathcal{E}} = -k^2 \mathcal{A}\,\vec{\mathcal{E}}, \quad \vec{\mathcal{E}} \rightsquigarrow \vec{\mathcal{E}}_\infty \text{ as } x \to -\infty, \tag{3.4}$$

where the coupling matrix is

$$\mathcal{A} = \mathbf{1}_3 + \frac{\Delta\epsilon}{\epsilon_\perp}\mathbf{n}\otimes\mathbf{n}. \tag{3.5}$$

Since at the postulated level of approximation we have $\mathbf{n} = \mathbf{n}(\rho,\phi) = \cos\theta(\rho)\mathbf{k} + \sin\theta(\rho)\boldsymbol{\phi}$, we are naturally led to express also the electric field as

$$\vec{\mathcal{E}} = \mathcal{E}_\rho(\rho,\phi,z)\,\boldsymbol{\rho} + \mathcal{E}_\phi(\rho,\phi,z)\,\boldsymbol{\phi} + \mathcal{E}_z(\rho,\phi,z)\,\mathbf{k}. \tag{3.6}$$

Then, it is easier to explicit the off-diagonal contributions to (3.4). Indeed, provided that

$$(\mathbf{n}\cdot\vec{\mathcal{E}})\mathbf{n} = (\sin\theta\,\mathcal{E}_\phi + \cos\theta\,\mathcal{E}_z)(\cos\theta\,\mathbf{k} + \sin\theta\,\boldsymbol{\phi}), \tag{3.7}$$

(3.4) reads

$$(\nabla^2 + k^2)(\mathcal{E}_\rho\,\boldsymbol{\rho} + \mathcal{E}_\phi\,\boldsymbol{\phi} + \mathcal{E}_z\,\mathbf{k})$$
$$= -k^2\frac{\Delta\epsilon}{\epsilon_\perp}[(\sin\theta\,\mathcal{E}_\phi + \cos\theta\,\mathcal{E}_z)\cos\theta\,\mathbf{k}$$
$$+ (\sin\theta\,\mathcal{E}_\phi + \cos\theta\,\mathcal{E}_z)\sin\theta\,\boldsymbol{\phi}]. \tag{3.8}$$
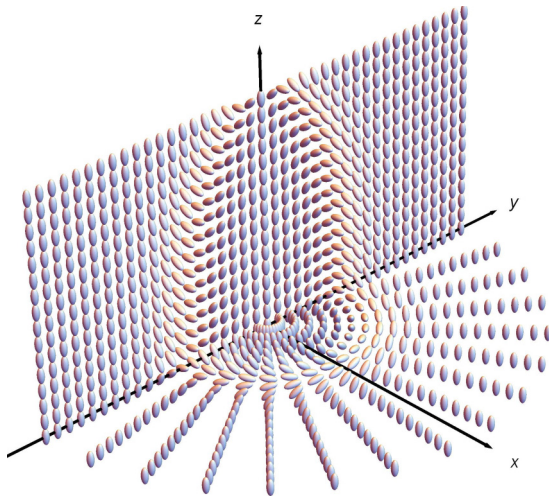

FIG. 5. Frontal and equatorial sections of the director field distribution for a spherulite in CLC. Here the parameters are the same as in Fig. 3(b), i.e., $\left(\frac{E}{E_0}\right) = 1.02$, $k_s = 6$, $\nu = 1.8$. Notice how the transversal radius of the spherulite decreases near the bounding plane surfaces.

However, now the Laplacian operator acts on the cylindrical components of a vector field, then it takes different expressions according to the component index. In particular, by defining $\nabla_0^2 \cdot = \frac{1}{\rho}\partial_\rho(\rho\,\partial_\rho \cdot) + \frac{1}{\rho^2}\partial_\phi^2 + \partial_z^2$, Eq. (3.8) becomes

$$\left(\nabla_0^2 + k^2\right)\mathcal{E}_\rho = \frac{1}{\rho^2}(\mathcal{E}_\rho + 2\,\partial_\phi\,\mathcal{E}_\phi), \tag{3.9}$$

$$\left(\nabla_0^2 + k^2\right)\mathcal{E}_\phi = \frac{1}{\rho^2}(\mathcal{E}_\phi - 2\,\partial_\phi\,\mathcal{E}_\rho)$$
$$- k^2\frac{\Delta\epsilon}{\epsilon_\perp}\left(\sin^2\theta\,\mathcal{E}_\phi + \frac{1}{2}\sin 2\theta\,\mathcal{E}_z\right), \tag{3.10}$$

$$\left(\nabla_0^2 + \tilde{k}^2\right)\mathcal{E}_z = -k^2\frac{\Delta\epsilon}{\epsilon_\perp}\left(\frac{1}{2}\sin 2\theta\,\mathcal{E}_\phi - \sin^2\theta\,\mathcal{E}_z\right). \tag{3.11}$$

In order to describe the scattering of the light on the spherulite, the above equations have to be solved under the asymptotic conditions

$$\mathcal{E}_\rho \rightsquigarrow \mathcal{E}_{\infty\rho}\sin\phi\,e^{\iota k\rho\cos\phi}, \quad \mathcal{E}_\phi \rightsquigarrow \mathcal{E}_{\infty\phi}\cos\phi\,e^{\iota k\rho\cos\phi},$$
$$\mathcal{E}_z \rightsquigarrow \mathcal{E}_{\infty z}e^{\iota\tilde{k}\rho\cos\phi} \quad \text{for } \phi \to \pm\pi \text{ and } \rho \to \infty. \tag{3.12}$$

Of course, such asymptotic conditions are exact solutions of the homogeneous system above, i.e., when $\frac{\Delta\epsilon}{\epsilon_\perp} \to 0$. As the problem of finding a complete analytical solution to (3.10) and (3.11) is quite hard, let us consider a perturbative setting. The basic idea is to first give a Born-approximated solution of Eq. (3.11), keeping an implicit dependence on $\mathcal{E}_\phi$. Then we can use it in (3.10) which will become a closed linear equation, even if nonlocal, in $\mathcal{E}_\phi$. Solving it, in the same approximation, one can use these results into (3.9) for $\mathcal{E}_\rho$ and finally solve it in the same scheme.

IV. PERTURBATIVE SOLUTIONS OF THE LIGHT-SCATTERING EQUATIONS BY A SPHERULITE

A. The *out-plane* conversion

Following the standard method by Lippmann-Schwinger [48], let us rewrite Eq. (3.11) as the integral equation

$$\mathcal{E}_z(\vec{r}) = \mathcal{E}_{\infty z}e^{\iota\tilde{k}\rho\cos\phi} + \int G(\vec{r},\vec{r}')U[\mathcal{E}_z(\vec{r}'),\mathcal{E}_\phi(\vec{r}'),\theta(\rho')]\,d\vec{r}', \tag{4.1}$$

where $U[\mathcal{E}_z(\vec{r}),\mathcal{E}_\phi(\vec{r}),\theta(\rho)] = -k^2\frac{\Delta\epsilon}{\epsilon_\perp}[\frac{1}{2}\sin 2\theta(\rho)\,\mathcal{E}_\phi(\vec{r}) - \sin^2\theta(\rho)\,\mathcal{E}_z(\vec{r})]$ and the Green function $G(\vec{r},\vec{r}')$ has the general form

$$G = \frac{1}{2\pi\nu}\sum_{m,n=-\infty}^{\infty} e^{\frac{2\pi\iota n}{\nu}(z-z')}e^{\iota m(\phi-\phi')}h_{m,n}(\rho,\rho'), \tag{4.2}$$

where the functions $h_{n,m}$ satisfy the Bessel-type equation with singular inhomogeneity [43]

$$\left[\frac{1}{\rho}\partial_\rho(\rho\,\partial_\rho \cdot) - \frac{m^2}{\rho^2} + \tilde{k}^2 - \left(\frac{2\pi n}{\nu}\right)^2\right]h_{m,n} = \frac{1}{\rho'}\delta(\rho-\rho'). \tag{4.3}$$

Thus, cutoff frequencies $\kappa_n = \sqrt{\tilde{k}^2 - \left(\frac{2\pi n}{\nu}\right)^2}$ are induced by the finite transverse size of the CLC layer.

We require G to be a continuous function with a bounded behavior at $\rho \to 0$ and, additionally, to be a cylindrical progressive wave as $\rho \to \infty$, i.e., of the form $\propto \frac{e^{\iota\kappa\rho}}{\sqrt{\kappa\rho}}$. Furthermore, G can have discontinuities only in the first derivatives at $\rho \to \rho'$.

Without further calculations, drastic simplifications stem from our assumption 5 in Sec. 3, implying that the only nonvanishing contributions come from the $n = 0$ mode. Moreover, we are actually interested in the behavior of the wave at radii much larger than the effective size of the spherulite, which decreases very fast, as we noticed in (2.14). Thus the form of Green function we have to use is

$$G_{\text{simpl}}(\vec{r},\vec{r}') = \frac{-\iota}{4}\sum_{m=-\infty}^{\infty} e^{\iota m(\phi-\phi')}H_m^{(1)}(\tilde{k}\,\rho)J_m(\tilde{k}\,\rho'), \tag{4.4}$$

where J_m denotes the Bessel function of first kind with integer order m and $H_m^{(1)}(\zeta) = J_m(\zeta) + \iota\,Y_m(\zeta)$ the corresponding Hankel function of first kind [43].

Now, replacing the above formula into (4.1), introducing the explicit form of the potential U, and considering the anisotropy ratio $\frac{\Delta\epsilon}{\epsilon_\perp}$ as a perturbation parameter, we express the wave function as a power series of it. At the 0 order the solution is given by asymptotics (3.12), which, replaced into (4.1), provides the first-order (Born approximation) corrections to the plane wave.

Thus, in the Born limit, by the identity $e^{\iota\zeta\cos p} = \sum_{l=-\infty}^{\infty} e^{\frac{\iota\pi l}{2}}e^{\iota l p}J_l(\zeta)$, one can integrate on ϕ' and obtain the approximated expression $\mathcal{E}_z^B(\vec{r})$ of the $\mathcal{E}_z(\vec{r})$ component, i.e.,

$$\mathcal{E}_z^B(\vec{r}) = \mathcal{E}_{\infty z}e^{\iota\tilde{k}\rho\cos\phi} + \frac{\pi}{2}\frac{\Delta\epsilon k^2}{\epsilon_\perp}\sum_{m=-\infty}^{\infty} e^{\iota m\phi}H_m^{(1)}(\tilde{k}\,\rho)$$
$$\times \int\left\{\mathcal{E}_{\infty\phi}\frac{\iota^m}{4}\sin[2\theta(\rho')]J_m(\tilde{k}\,\rho')\right.$$
$$\times [J_{m-1}(k\,\rho') - J_{m+1}(k\,\rho')]$$
$$\left. - \mathcal{E}_{\infty z}\iota^{m+1}\sin^2[\theta(\rho')]J_m^2(\tilde{k}\,\rho')\right\}\rho'd\rho'. \tag{4.5}$$

In order to have a simple estimation of the integrals in the above expression, let us resort to the asymptotic expressions of the spherulite given by (2.12) and (2.16). Actually, the simplest rough choice is (2.13) [with $Z(z) = 1$], which we will adopt here in order to estimate the more relevant contributions to the scattering amplitudes. Thus, we have to evaluate integrals of the form

$$\mathcal{I}_m^\phi = -\int_0^{\pi k\rho_0}\sin\left(2\frac{s}{k\rho_0}\right)J_m(s)[J_{m-1}(s) - J_{m+1}(s)]\,s\,ds$$
$$= -\int_0^{\pi k\rho_0}\sin\left(2\frac{s}{k\rho_0}\right)[J_m(s)^2]'\,s\,ds, \tag{4.6}$$

$$\mathcal{I}_m^z = \int_0^{\pi k\rho_0}\sin^2\left(\frac{s}{k\rho_0}\right)J_m^2(s)\,s\,ds, \tag{4.7}$$

where the substitution $\tilde{k} \to k$ is justified, since a further correction of the order $\frac{\Delta\epsilon}{\epsilon_\perp}$ is introduced.

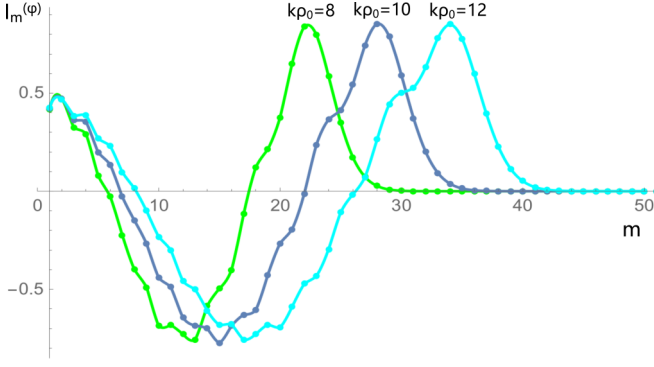FIG. 6. The numerical values of $\mathcal{I}_m^\phi$ as function of $0 \leqslant m \leqslant 50$ for three different values of $k\rho_0 = 8, 10, 12$. They can be approximated by continuous functions in m, for instance, by linear combinations of Gaussian functions but still a clear pattern for a systematic approximation has to be developed. It is evident a linear dependence, with a slope ~ 4, on the number of significant terms with the size parameter $k\rho_0$. This is in agreement with the scattering features on localized central potentials.

At the moment the above matrix elements do not have yet an analytical expression and should be computed numerically.

Examples of the numerical evaluation of a certain number of integrals (4.6) is given in Fig. 6.

Before proceeding in such a calculation let us show the form of the cross section of conversion of a *in plane* polarized wave into a *out plane* polarized one. In fact, if we suppose $\mathcal{E}_{\infty z} = 0$, then the scattered amplitude along the z axis (4.5) reads

$$\mathcal{E}_z^B(\vec{r}) = \mathcal{E}_{\infty\phi} \frac{\pi \, \Delta\epsilon}{8 \, \epsilon_\perp} \sum_{m=-\infty}^{\infty} \iota^m \, \mathcal{I}_m^\phi \, e^{im\phi} \, H_m^{(1)}(\tilde{k}\,\rho).$$

Recalling that at infinity the asymptotic behavior of the Hankel functions is $H_m^{(1)}(\zeta) \rightsquigarrow \frac{(1-i)e^{i\zeta - \frac{i\pi m}{2}}}{\sqrt{\pi \zeta}} + O(\zeta^{-3/2})$, the above
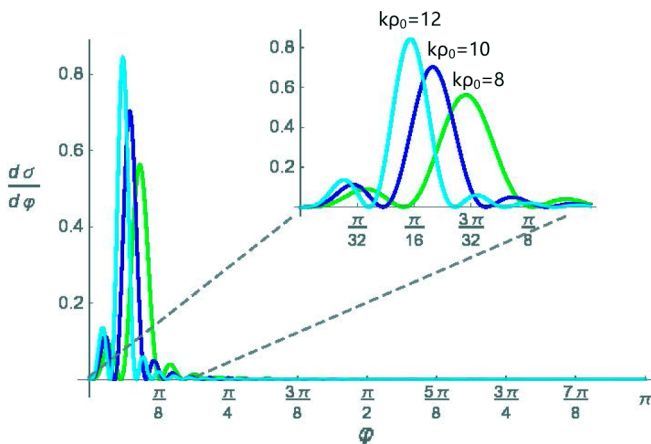

FIG. 7. The numerical evaluation of the conversion cross section (4.9), in arbitrary units, for the three different values of $k\rho_0$ used in Fig. 6.

expression becomes

$$\mathcal{E}_z^B(\vec{r}) = (1-\iota)\,\mathcal{E}_{\infty\phi} \frac{\pi \, \Delta\epsilon}{8 \, \epsilon_\perp} \frac{e^{\iota \tilde{k}\rho}}{\sqrt{\pi \, \tilde{k}\,\rho}} \left(\mathcal{I}_0^\phi + 2\sum_{m=1}^{+\infty} \mathcal{I}_m^\phi \, \cos m\phi \right),$$
(4.8)

where the identity $\mathcal{I}_{-m}^\phi = \mathcal{I}_m^\phi$ holds because $J_{-m} = (-1)^m J_m$. Now, it is clear that a sufficient condition for (4.8) to be a good approximation is that $\mathcal{E}_z$ be small also in the core region delimited by $\rho \leqslant \rho_0$, where the integral in (4.1) receives significant contributions. Thus, taking into account the behavior of the Green functions around the origin, we conclude that we must have $\pi k^{3/2} |\frac{\Delta\epsilon}{\epsilon_\perp}| \int_0^{\pi \rho_0} \rho^{1/2} |\sin 2\theta(\rho)| \, d\rho \leqslant \frac{2}{3}\pi^{5/2} |\frac{\Delta\epsilon}{\epsilon_\perp}| \, (k\,\rho_0)^{3/2} << 1$, which provides a bounding relationship between the size parameter and the relative anisotropy.

The cross section of the conversion of linear *in plane* polarized $\hat{y}$ light into the *out plane* $\hat{z}$ one is given by

$$\frac{d\sigma}{d\phi}(\hat{r}, \hat{k}; \hat{i}, \hat{j}) = \frac{\pi}{32} \sqrt{\frac{\epsilon_\perp}{\epsilon_\parallel}} \left(\frac{\Delta\epsilon}{\epsilon_\perp}\right)^2 \frac{\nu \, \rho_0}{k \, \rho_0}$$
$$\times \left(\mathcal{I}_0^\phi + 2\sum_{m=1}^{+\infty} \mathcal{I}_m^\phi \, \cos m\phi \right)^2, \quad (4.9)$$

where we have singled out the dependence on the geometrical size of the spherulites, i.e., the area $\nu \, \rho_0$, from its relative size parameter $k \, \rho_0$ with respect the used light wavelength. Thus a residual dependency on the static external field E/E_0 is still present in the above function.

The calculations of the conversion cross section in the direction $\hat{r}(\phi)$ indicates that there is a quite well-defined small angle, around $10°$ in our numerical examples (Fig. 7), within which the rotation of the polarization is efficiently performed. The angle of maximum conversion is $\propto (k\rho_0)^{-1}$, thus it becomes smaller as the wavelength becomes shorter. The backscattering cross section is a quite regular function slowly decreasing as $k \, \rho_0$ increases. This dependency on $k \, \rho_0$ can be related to the well-known CLCs property of selective reflection within a specific bandwidth, depending on the material parameters q_0, $\epsilon_\parallel$, $\epsilon_\perp$ [19]. The effective value of the scattering cross section depends basically on the square of the anisotropy ratio $\left(\frac{\Delta\epsilon}{\epsilon_\perp}\right)^2$. Actually the total cross section takes the expression

$$\sigma(\hat{k}, \hat{j}) = \frac{\pi^2}{16} \sqrt{\frac{\epsilon_\perp}{\epsilon_\parallel}} \left(\frac{\Delta\epsilon}{\epsilon_\perp}\right)^2 \frac{\nu \, \rho_0}{k\rho_0} \left[(\mathcal{I}_0^\phi)^2 + 2\sum_{m=1}^{\infty} (\mathcal{I}_m^\phi)^2 \right],$$
(4.10)

which is a decreasing function of the size parameter $k \, \rho_0$.

Let us turn our attention again to Eq. (4.5). By using the numerical solutions for the spherulite (Figs. 3 and 4), we can obtain a more accurate evaluation of the differential cross section in (4.9), for the scattering of an electromagnetic wave by a skyrmion. A direct comparison between the differential cross sections, computed with the use of the numerical and the approximated solutions, is reported in Figs. 8 and 9 in arbitrary units. As it can be seen, the numerical solution for the spherulites makes the angle of maximum conversion smaller than the one computed through the use of the approximated
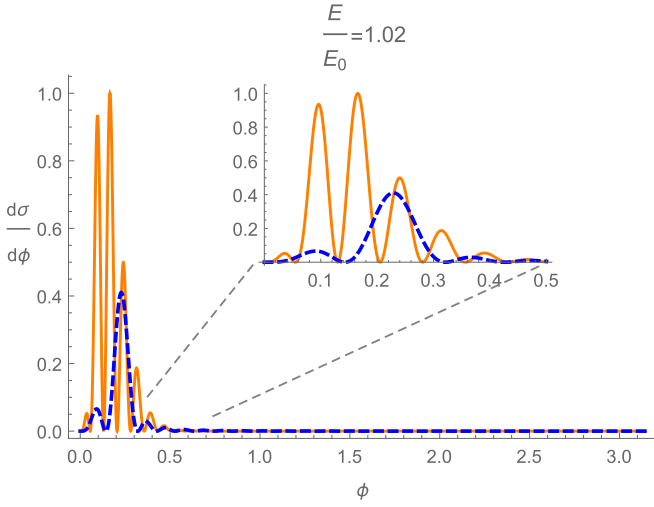
FIG. 8. The numerical evaluation of the conversion cross section (4.9), in arbitrary units, for ρ_0 fixed by (2.11) and the ratio $E/E_0 = 1.02$, $k\rho_0 = 10$, for the numerical solution (solid line) and the approximated solution (2.12) (dashed line).

solution. Furthermore, recalling that as the external electric field increases, the size of the spherulite decreases [as described by Eq. (2.11)], we note that the larger the size of the skyrmion is, the more efficient the polarization conversion is with respect to the approximated one.

B. The *in-plane* conversion

Assuming $\mathcal{E}_{\infty\rho} = \mathcal{E}_{\infty\phi} = 0$, let us turn our attention to the subsystem (3.9) and (3.10), which could be represented in the form

$$
\begin{pmatrix} L + k^2 & -M \\ M & L + k^2 \end{pmatrix} \begin{pmatrix} \mathcal{E}_\rho \\ \mathcal{E}_\phi \end{pmatrix}
$$
$$
= k^2 \frac{\Delta\epsilon}{\epsilon_\perp} \begin{pmatrix} 0 \\ \sin^2\theta\, \mathcal{E}_\phi + \frac{1}{2}\sin 2\theta\, \mathcal{E}_z \end{pmatrix}, \qquad (4.11)
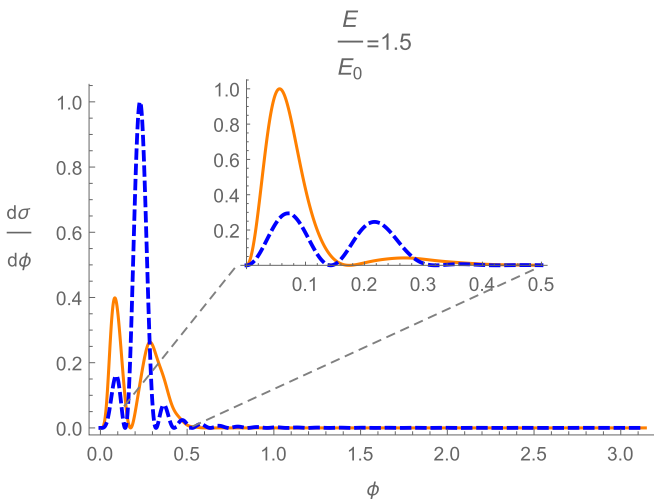$$

FIG. 9. The numerical evaluation of the conversion cross section (4.9), in arbitrary units, for ρ_0 fixed by (2.11) and the ratio $E/E_0 = 1.5$, $k\rho_0 = 10$, for the numerical solution (solid line) and the approximated solution (2.12) (dashed line).

where $L = \nabla_0^2 - \frac{1}{\rho^2}$ and $M = \frac{2}{\rho^2}\partial_\phi$. Following the same reasoning as above, we limit ourselves to evaluating the scattering of light by the spherulite in the Born approximation. Accordingly, the conversion from out-plane to in-plane polarized light scattering leads to the following approximated expression:

$$
\begin{pmatrix} \mathcal{E}_\rho^B \\ \mathcal{E}_\phi^B \end{pmatrix} = \mathcal{E}_{\infty z}\, \frac{k^2}{2\pi\nu} \frac{\Delta\epsilon}{2\,\epsilon_\perp}
$$
$$
\times \sum_{m,n=-\infty}^{\infty} \int \sin 2\theta(\rho')\, e^{\imath \bar{k}\rho'\cos\phi'}\, e^{\frac{2\pi\imath n}{\nu}(z-z')}\, e^{\imath m(\phi-\phi')}
$$
$$
\times \begin{bmatrix} -\imath\, f_{m,n}(\rho,\rho') \\ h_{m,n}(\rho,\rho') \end{bmatrix} d\vec{r}', \qquad (4.12)
$$

where $h_{m,n}$ and $f_{m,n}$ are solutions of a suitable differential system (see below). Again, using the simplification induced by the assumption 5 in Sec. 3 and by using the expansion of the plane wave factor in terms of Bessel functions, one gets

$$
\begin{pmatrix} \mathcal{E}_\rho^B \\ \mathcal{E}_\phi^B \end{pmatrix} = \mathcal{E}_{\infty z}\, \frac{\Delta\epsilon\, k^2}{2\,\epsilon_\perp} \sum_{m=-\infty}^{\infty} \imath^m\, e^{\imath m\phi} \int \sin 2\theta(\rho')\, J_m(\bar{k}\rho')
$$
$$
\times \begin{bmatrix} -\imath\, f_m(\rho,\rho') \\ h_m(\rho,\rho') \end{bmatrix} \rho'\, d\rho', \qquad (4.13)
$$

where we dropped the subscript n from both $h_{m,n}$ and $f_{m,n}$ as the only nonvanishing contributions come from the $n=0$ mode. The squared modulus of the above quantity, properly managed, will produce the cross section of the *out-plane–in-plane* scattering process.

The equations for h_m and f_m are as follows:

$$
h_m''(\rho) + \frac{h_m'(\rho)}{\rho} + \left(k^2 - \frac{m^2+1}{\rho^2}\right)h_m(\rho) + \frac{2m f_m(\rho)}{\rho^2} = \frac{\delta(\rho-\rho')}{\rho'},
$$
$$
f_m''(\rho) + \frac{f_m'(\rho)}{\rho} + \left(k^2 - \frac{m^2+1}{\rho^2}\right)f_m(\rho) + \frac{2m h_m(\rho)}{\rho^2} = 0. \qquad (4.14)
$$

The general solution of the system above is

$$
h_m^{\pm} = c_1^{\pm} J_{m-1}(k\rho) + \imath c_2^{\pm} Y_{m-1}(k\rho)
$$
$$
+ d_1^{\pm} J_{m+1}(k\rho) + \imath d_2^{\pm} Y_{m+1}(k\rho),
$$
$$
f_m^{\pm} = c_1^{\pm} J_{m-1}(k\rho) + \imath c_2^{\pm} Y_{m-1}(k\rho)
$$
$$
- d_1^{\pm} J_{m+1}(k\rho) - \imath d_2^{\pm} Y_{m+1}(k\rho), \qquad (4.15)
$$

where (c_i^-, d_i^-) and (c_i^+, d_i^+) are two quadruples of arbitrary constants in the regions $\rho < \rho'$ or $\rho > \rho'$, respectively. Continuity of the solutions and discontinuity of their first derivatives at ρ' imply a functional dependence of those coefficients on this variable. Moreover, as in the previous section, we require regularity at $\rho \to 0$ and radiative behavior at $\rho \to \infty$.

All conditions above lead to a linear system, from which one obtains the values of the unknown coefficients, namely

$$
c_1^+ = -\frac{\imath\pi}{4} H_{m-1}^{(1)}(k\rho'),
$$
$$
d_1^+ = -\frac{\imath\pi}{4} H_{m+1}^{(1)}(k\rho'),\ \ c_2^+ = d_2^+ = 0,
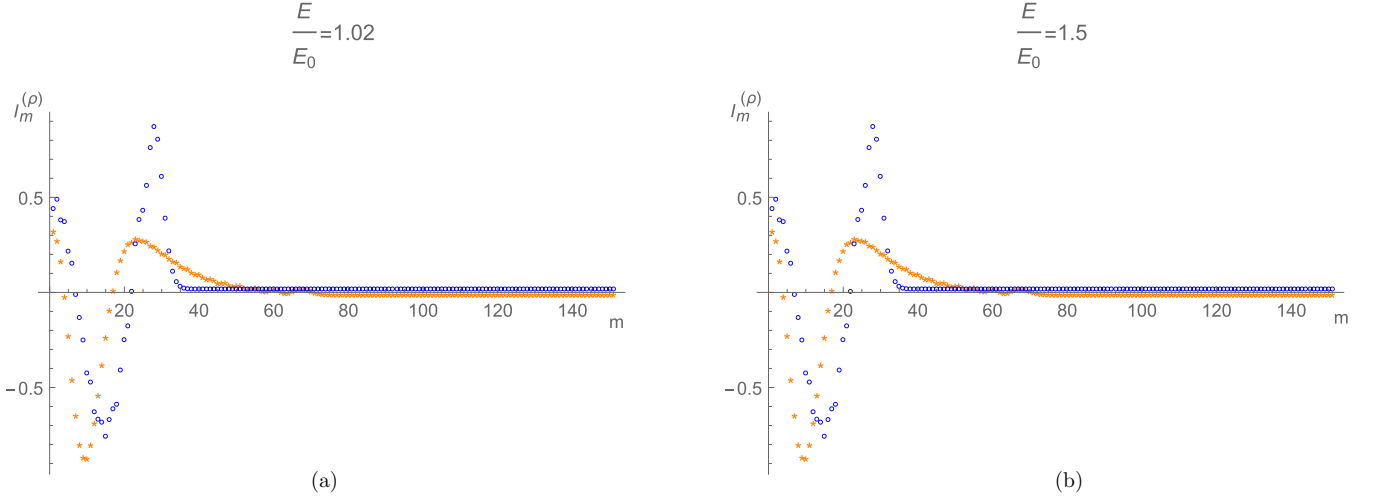$$

FIG. 10. The numerical values of $I_m^{(\rho)}$ as function of $0 \leqslant m \leqslant 150$, for two different values of E/E_0 with fixed $k\rho_0$, computed through the use of the numerical solution (stars) and the approximated solution (2.12) (circles).

$$c_1^- = c_2^- = -\frac{\iota \pi}{4} J_{m-1}(k \rho'),$$

$$d_1^- = d_2^- = -\frac{\iota \pi}{4} J_{m+1}(k \rho'). \tag{4.16}$$

Now we are in position to evaluate (4.13), namely

$$\frac{\mathcal{E}_{\infty z} \sqrt{\pi} \, \Delta\epsilon \, k^2}{2^{\frac{5}{2}} \epsilon_\perp} e^{-\iota \frac{\pi}{4}} \frac{e^{\iota k \rho}}{\sqrt{k \rho}} \sum_{m=-\infty}^{\infty} e^{\iota m \phi} \int \sin 2\theta(\rho') \, J_m(\tilde{k}\rho')$$

$$\times \left\{ \begin{array}{c} -\iota \left[J_{m-1}(k \rho') + J_{m+1}(k \rho') \right] \\ J_{m-1}(k \rho') - J_{m+1}(k \rho') \end{array} \right\} \rho' \, d\rho'. \tag{4.17}$$

Setting

$$\frac{1}{\tilde{k}^2} I_m^{(\rho)} = \frac{1}{k^2} \int \sin 2\theta \left(\frac{s}{\tilde{k}} \right) J_m(s)$$

$$\times \left[J_{m-1} \left(k \frac{s}{\tilde{k}} \right) + J_{m+1} \left(k \frac{s}{\tilde{k}} \right) \right] s \, ds \, d\phi' \tag{4.18}$$

$$\frac{1}{\tilde{k}^2} I_m^{(\phi)} = \frac{1}{k^2} \int \sin 2\theta \left(\frac{s}{\tilde{k}} \right) J_m(s)$$

$$\times \left[J_{m-1} \left(k \frac{s}{\tilde{k}} \right) - J_{m+1} \left(k \frac{s}{\tilde{k}} \right) \right] s \, ds, \tag{4.19}$$

Eq. (4.17) can be rewritten as

$$\frac{\mathcal{E}_{\infty z} \sqrt{\pi} \, \Delta\epsilon}{2^{\frac{5}{2}} \epsilon_\perp} e^{-\iota \frac{\pi}{4}} \frac{e^{\iota k \rho}}{\sqrt{k \rho}} \sum_{m=-\infty}^{\infty} e^{\iota m \phi} \left[\begin{array}{c} -\iota \, I_m^{(\rho)} \\ I_m^{(\phi)} \end{array} \right]. \tag{4.20}$$

Recalling the identity $J_{-m} = (-1)^m J_m$, it is easy to show that $I_0^{(\rho)} = 0$, $I_m^{(\rho)} = -I_{-m}^{(\rho)}$, and $I_m^{(\phi)} = I_{-m}^{(\phi)}$, so that Eq. (4.20) now reads

$$\frac{\mathcal{E}_{\infty z} \sqrt{\pi} \, \Delta\epsilon}{2^{\frac{5}{2}} \epsilon_\perp} e^{-\iota \frac{\pi}{4}} \frac{e^{\iota k \rho}}{\sqrt{k \rho}} \left[\begin{array}{c} 2 \sum_{m=1}^{\infty} I_m^{(\rho)} \sin m\phi \\ I_0^{(\phi)} + 2 \sum_{m=1}^{\infty} I_m^{(\phi)} \cos m\phi \end{array} \right]. \tag{4.21}$$

Performing again the substitution $\tilde{k} \to k$, we notice that $I_m^{(\phi)}$ is the same as $\mathcal{I}_m^\phi$ in Eq. (4.6). On the other hand, the values of the first 300 matrix elements (4.18) are presented in Fig. 10.

The *in plane-conversion* cross section is then given by

$$\frac{d\sigma}{d\phi}(\hat{r}, \hat{\phi}; \hat{i}, \hat{j}, \hat{k})$$

$$= \frac{\pi}{32} \sqrt{\frac{\epsilon_\perp}{\epsilon_\parallel}} \left(\frac{\Delta\epsilon}{\epsilon_\perp} \right)^2 \frac{\nu \rho_0}{k \rho_0} \left\{ 4 \left[\sum_{m=1}^{\infty} I_m^{(\rho)} \sin m\phi \right]^2 \right.$$

$$\left. + \left[I_0^{(\phi)} + 2 \sum_{m=1}^{+\infty} I_m^{(\phi)} \cos m\phi \right]^2 \right\} \tag{4.22}$$
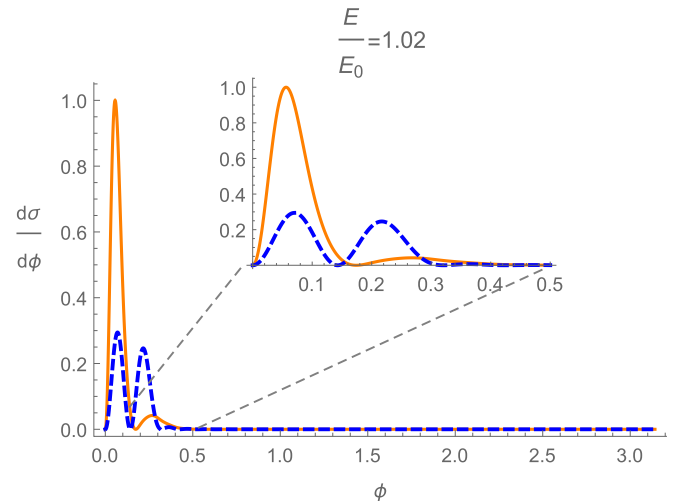

FIG. 11. The numerical evaluation of the conversion cross section (4.22), in arbitrary units, for $E/E_0 = 1.02$ and $k\rho_0 = 10$. The numerical solution corresponds to the solid line and the approximated solution (2.12) to the dashed one.
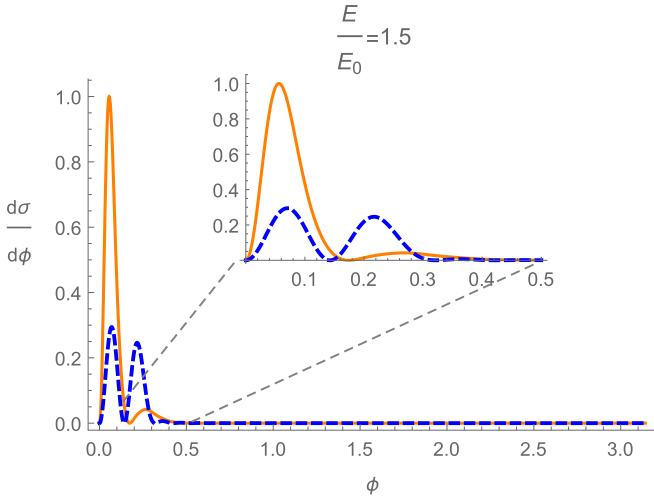
FIG. 12. The numerical evaluation of the conversion cross section (4.22), in arbitrary units, for $E/E_0 = 1.02$ and $k\rho_0 = 10$. The numerical solution corresponds to the solid line and the approximated solution (2.12) to the dashed one.

and the total cross section reads

$$
\sigma(\hat{\phi}, \hat{k}) = \frac{\pi^2}{16} \sqrt{\frac{\epsilon_\perp}{\epsilon_\parallel}} \left(\frac{\Delta\epsilon}{\epsilon_\perp} \right)^2 \frac{v\,\rho_0}{k\,\rho_0} \left\{ \left[I_0^{(\phi)} \right]^2 \right.
$$
$$
\left. + 2 \sum_{m=1}^{\infty} \left[I_m^{(\rho)} \right]^2 + 2 \sum_{m=1}^{+\infty} \left[I_m^{(\phi)} \right]^2 \right\}. \quad (4.23)
$$

The numerical results, in arbitrary units, for the computation of the differential cross section (4.22) are depicted in Figs. 11 and 12 for two different values of the ratio E/E_0. Conversely to what happens for the *out-plane* conversion cross section, in

this case the use of the numerical solution for the computation of the differential cross section (4.22) keeps the angle of maximum conversion substantially unchanged.

The same results are represented as a log-polar plot in Fig. 13 for the choice of the size parameter $k\rho_0 = 10$. The plots are referred to certain suitably chosen units. Both approximated linear (dashed line) and numerical (solid line) solutions for the skyrmion are presented for two different values of the electric field. Of course, since our calculations were performed considering an incident light beam on an object of variable refractive index in a localized region and rapidly tending to a constant asymptotic value, the scattering cross sections look very similar to those obtained for the light scattering by water or nematic droplets in the Mie regime. In particular, our cross sections share some common properties with those obtained in the Rayleigh-Gans approximation for nematic droplets [49,50]. In fact, our results are in good agreement with those reported in Fig. 3(c) of Ref. [49] for an aligned polymer-dispersed liquid crystal (PDLC) droplet, except for the presence of a significant backscattering. On the other hand, the dependence of the cross section on the incident light wavelength is similar to ours, i.e., the angle of maximum conversion becomes smaller as the wavelength decreases. The size parameter ranges in an intermediate interval of the magnitude $O(1)$. As for a comparison with the water droplet scattering, the first striking difference is the absence of a prominent main lobe at $0°$. On the contrary the strong direct forward transmission is replaced by a dip between two side lobes, one order of magnitude larger. The angular position of the first side lobes increases with the intensity of the applied electric field. Recalling that actually we are looking for the scattered light with an orthogonal polarization with respect to the incident one, limiting the angle within $\sim \pm 30°$, Fig. 13 provides a computed intensity distribution as observed at the eyepiece of a polarizing microscope. An
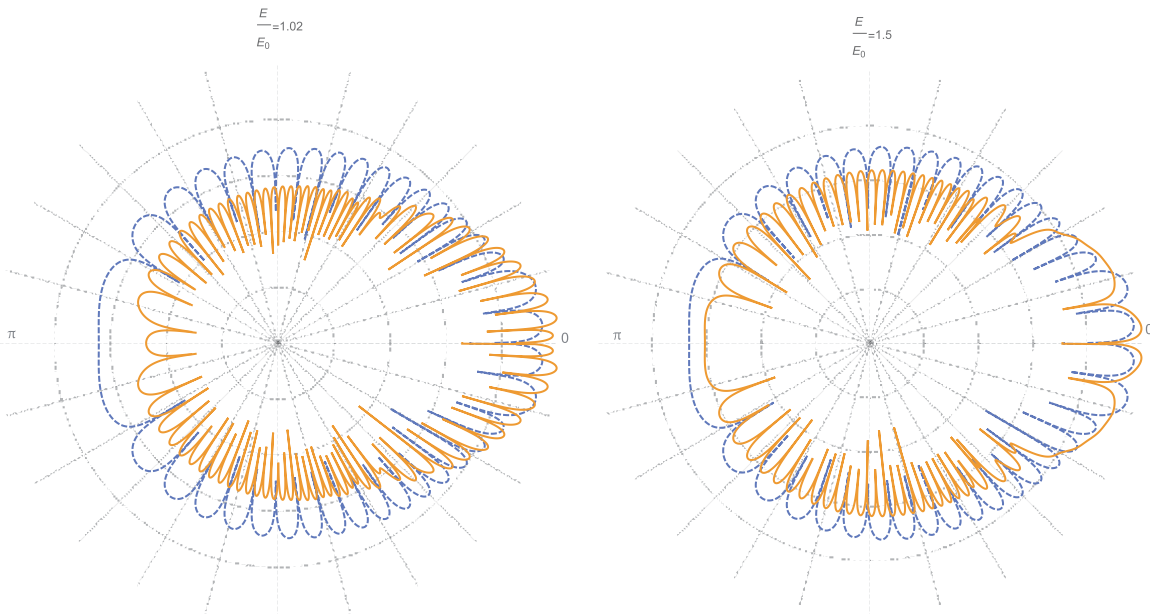

FIG. 13. Comparison of the log-polar plots of the in-plane–out-plane conversion differential cross sections for two different values of the external electric field. In both cases the solid line curves refer to the numerical spherulite profile, while the dashed ones correspond to the piecewise linear approximation of it.
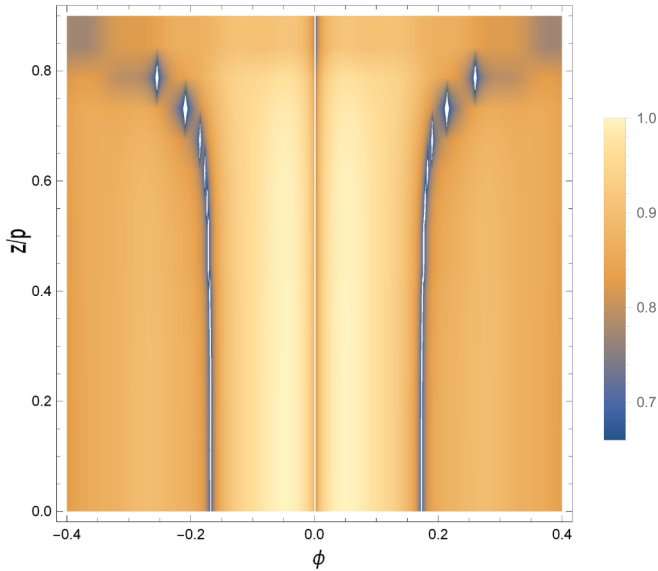
FIG. 14. The density plot has been obtained computing the cross section (4.22) at different values of $0 \leqslant z \leqslant \frac{1}{2} L/p$, $k\rho_0 = 10$ and $E/E_0 = 1.5$, without any modification in (4.22) but changing the spherulite radius accordingly to $\rho_0 Z(z)$ in (2.13) and (2.14).

attempt to reproduce such distribution is reported in Fig. 14 as a density plot. This plot has been obtained by computing the cross section (4.22) at different values of $0 \leqslant z \leqslant \frac{1}{2} L/p$, without any modification in (4.22) but changing the spherulite radius accordingly to $\rho_0 Z(z)$ in (2.13) and (2.14). Thus, the two side lobes are clearly visible. But the secondary minima become more and more distant as z approaches the upper bounding surface. This is the opposite of what one can see in the pictures in Ref. [27]. The reason is quite simple: Actually, we are considering a sequence of scattering cross sections of infinitely long cylinders of decreasing radii. That, of course, implies a corresponding increase of the angular positions of the minima. To improve such a result we should consider the diffraction by an anisotropic ellipsoidal-like obstacle [51,52].

A further interesting feature of the plots in Fig. 13 is the presence of a significant lobe at π, of the same order in magnitude, or larger than, as the two closest side lobes. As opposed to the case of the water droplet, they are not strong enough and well distinct from the backward reflection coefficient to assure a significant visibility to a rainbow. This effect should be easily observed by the experimentalists.

V. CONCLUSIONS

In the present work we showed that the spherulites in CLC can be used to change the polarization axes of incoming light with a certain efficiency. To the best of our knowledge, this phenomenon is quite new. In detail we first described the shape of the spherulites for different values of the controlling parameters, in particular the external applied electric (or magnetic) field. From that we have been able to compute the cross

section of the polarization axes conversions in Born approximation. We found that the conversion processes have maximum differential cross section at small nonzero deflection angles. Thus, the effect we described can be detected off the forward direction. Furthermore, we compared the differential cross sections for different values of the external electric field, proving that the scattering is significantly influenced by such a parameter. Thus, we can use it as a tuning controller of the scattering. In particular, the conversion is more efficient for fields above the threshold of the critical unwinding field of the cholesteric-nematic transition. This is due to the quadratic inverse dependence on the external field of the spherulite core size. In order to obtain these results, we used both a piecewise linear approximation of the spherulite profile and the corresponding numerical solution. On the other hand, we showed that the spherulite is badly approximated by a piecewise linear function, especially for electric fields near to E_0. Actually, there are many questions to be answered. First, it would be important to study the cross sections for all channels, beyond the Born approximation, and to suppress the several simplifications we made. In particular, the spherulite is not a cylinder, as we assumed in the present work, but it resembles a barrel. Correspondingly, new diffractive effects may arise from the actual shape, especially close the confining plates. This is related to the type of anchoring, which is parametrized by a further controlling parameter in the Rapini-Papoular conditions. In fact, we showed that the shape of the spherulite depends significantly on it, even if the ratio E/E_0 is kept fixed. Second, as stated in Sec. 2 around Eq. (2.6), we assumed here that the azimuthal angle ψ depends only on ϕ. More complex dependence are to be considered as in Ref. [25], where the authors take into account the effect of additional dependence on ρ and z. Finally, it is well known that in specific ranges for the values of the model parameters lattice configurations of spherulites can appear [13,26]. This fact suggests to explore the light-scattering processes in such a regime in order to enhance the effects we described above or to have better control of them. Also, in the near future we are planning to extend the results obtained in this paper to the study of light interaction with a lattice of skyrmions. The results in the case of skyrmion lattices may be exploited eventually in designing switchable micromirrors and optical filters by photonic band gap materials based on CLC's. In such a field several current investigations concern the scattering of polarized light by localized and helicoidal structures, as suggested in Refs. [53,54]. Moreover, localized defects in CLCs, topologically stabilized and electrically controlled, may provide functional substrates for dispersed nanoparticles [55].

[1] G. Luckhurst, D. Dunmur, in *Liquid Crystals* in *Springer Handbook of Electronic and Photonic Materials*, edited by S. Kasap and P. Capper (Springer, Cham, 2017).

[2] G. V. Chigrinov, Front. Optoelectron. Chin. **3**, 103 (2010).

[3] H. Coles and S. Morris, Nat. Photon. **4**, 676 (2010).

[4] J. Beeckman and K. Neyts and P. J. M. Vanbrabant, Opt. Eng. **50**, 081202 (2011).

[5] P. Oswald and J. Baudry and S. Pirkl, Phys. Rep. **337**, 67 (2000).

[6] H. S. Kitzerow and P. P. Crooker, Liq. Cryst. **11(4)**, 561 (1992).

[7] D. K. Yang and P. P. Crooker, Liq. Cryst. **9**, 245 (1991).

[8] D. L. Patel, and D. B. Dupré, J. Polym. Sci., Polym. Phys. Ed. **18**, 1599 (1980).

[9] G. Assanto and N. F. Smyth, IEEE J. Sel. Top. Quantum Electron. **22**, 4400306 (2016).

[10] C. Carboni and A. K. George and A. Al-Lawati, Mol. Cryst. Liq. Cryst. **410**, 1109 (2004).

[11] P. J. Ackerman, Z. Qi, and I. Smalyukh, Phys. Rev. E **86**, 021703 (2012).

[12] P. J. Ackerman, Z. Qi, Y. Lin, C. W. Twombly, M. J. Laviada, Y. Lansac, and I. Smalyukh, Sci. Rep. **2**, 414 (2012).

[13] A. O. Leonov, I. E. Dragunov, U. K. Rößler, and A. N. Bogdanov, Phys. Rev. E **90**, 042502 (2014).

[14] G. De Matteis, L. Martina, and V. Turco, Theor. Math. Phys. **196** (2018).

[15] N. Romming, C. Hanneken, M. Menzel, J. E. Bickel, B. Wolter, K. von Bergmann, A. Kubetzka, and R. Wiesendanger, Science **341**, 6146 (2013).

[16] A. N. Bogdanov and U. K. Rößler, Phys. Rev. Lett. **87**, 037203 (2001).

[17] P. De Gennes and J. Prost, *The Physics of Liquid Crystals*, (Clarendon Press, Oxford, 1993).

[18] I. W. Stewart, *The Static and Dynamic Continuum Theory of Liquid Crystals: A Mathematical Introduction*, (Taylor & Francis, London, 2004).

[19] P. Oswald, P. Pieranski, G. Gray, and J. Goodby, *Nematic and Cholesteric Liquid Crystals*, (CRC Press, Boca Raton, FL, 2006).

[20] R. D. Kamien and J. V. Selinger, J. Phys.: Condens. Matter **13**, R1 (2001).

[21] T. Akahane and T. Tako, Jpn. J. Appl. Phys. **15**, 1559 (1976).

[22] B. Kerllenevich and A. Coche, Mol. Cryst. Liq. Cryst. **68**, 47 (1981).

[23] J. Baudry and S. Pirkl and P. Oswald, Phys. Rev. E **57**, 3038 (1998).

[24] P. Oswald and A. Dequidt, and A. Zywocinski, Phys. Rev. E **77**, 061703 (2008).

[25] S. Afghah and J. V. Selinger, Phys. Rev. E **96**, 012708 (2017).

[26] J. Fukuda and S. Zumer, Nat. Commun. **2**, 246 (2011).

[27] P. J. Ackerman, R. P. Trivedi, B. Senyuk, J. van de Lagemaat, and I. I. Smalyukh, Phys. Rev. E **90**, 012505 (2014).

[28] A. Nych, J. Fukuda, U. Ognysta, S. Zumer, and I. Musevic, Nat. Phys. **13**, 1215 (2017).

[29] G. Posnjak, S. Copar, and I. Musevic, Sci. Rep. **6**, 26361 (2016).

[30] I. Dierking, F. Giesselmann, P. Zugenmaier, Z. Naturforsch. A **50**, 589 (1995).

[31] N. Gheorghiu and G. Y. Panasyuk, arXiv:1705.02683 (2017).

[32] E. M. Therézio, S. F. C. da Silva, G. G. Dalkiranis, P. A. Filho, G. C. Santos, F. Ely, I. H. Bechtold, and A. Marletta, Opt. Mater. **48**, 7 (2015).

[33] P. Sleczkowski, Y. Zhou, S. Iamsaard, J. J. de Pablo, N. Katsonis, and E. Lacaze, Proc. Natl. Acad. Sci. USA **115**, 4334 (2018).

[34] R. Balamurugan and J. Liu, React. Funct. Polym. **105**, 9 (2016).

[35] J. Fukuda and S. Zumer, Opt. Express **26**, 1174 (2018).

[36] A. Rapini and M. Papoular, J. Phys. Colloq **30**, C4 (1969).

[37] P. J. Kedney and I. W. Stewart, Lett. Math. Phys. **31**, 261 (1994).

[38] N. Manton and P. Sutcliffe, *Topological Solitons*, 1st ed. (Cambridge University Press, Cambridge, 2004).

[39] A. A. Belavin and A. M. Polyakov, JETP Lett. **22**, 245 (1975).

[40] A. Barone and F. Esposito and C. J. Magee and A. C. Scott, Riv. Nuovo Cimento **1**, 227 (1971).

[41] M. J. Ablowitz and P. A. Clarkson, *Solitons, Nonlinear Evolution Equations and Inverse Scattering* (Cambridge University Press, Cambridge, 1991).

[42] B. M. McCoy and C. A. Tracy, and T. T. Wu, Painleve Functions of the third kind, J. Math. Phys. **18** (1977).

[43] NIST Digital Library of Mathematical Functions, http://dlmf.nist.gov/.

[44] William H. Press and A. Saul, *Numerical Recipes*, 3rd ed. (Cambridge University Press, Cambridge, 2007).

[45] R. J. LeVeque, *Finite Difference Methods for Ordinary and Partial Differential Equations: Steady-State and Time-Dependent Problems* (Society for Industrial and Applied Mathematics, Philadelphia, PA, 2007).

[46] J. D. Jackson, *Classical Electrodynamics*, 3rd ed. (Wiley, New York, 2012).

[47] M. Kleman, O. D. Lavrentovich, and J. Goodby, *Soft Matter Physics: An Introduction*, (Springer-Verlag, New York, 2003).

[48] B. A. Lippmann and J. Schwinger, Phys. Rev. **79**, 469 (1950).

[49] E. E. Kriezis, Microw. Opt. Technol. Lett. **35** (2002).

[50] Z. M. Wang, *Nanodroplets* (Springer, Berlin, 2013).

[51] R. Borghi, J. Opt. Soc. A **31**, 2120 (2014).

[52] P. Mazzeron and S. Muller, Appl. Opt. **35**, 3726 (1996).

[53] W. Cao, A. Muñoz, P. Palffy-Muhoray, B. Taheri, Nat. Mater. **1**, 111 (2002).

[54] I. I. Smalyukh, Y. Lansac, N. A. Clark, and R. P. Trivedi, Nat. Mater. **9**, 139 (2009).

[55] C. Blanc, D. Coursault, and E. Lacaze, Liq. Cryst. Rev. **1**, 1 (2013).